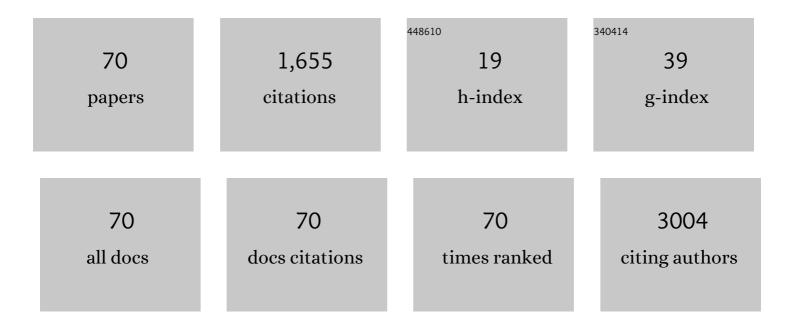
List of Publications by Year in descending order

Source: https://exaly.com/author-pdf/2129688/publications.pdf Version: 2024-02-01



HYUN-YONG YU

#	Article	IF	CITATIONS
1	Performance Analysis on Complementary FET (CFET) Relative to Standard CMOS With Nanosheet FET. IEEE Journal of the Electron Devices Society, 2022, 10, 78-82.	1.2	17
2	Analytical Model of Contact Resistance in Vertically Stacked Nanosheet FETs for Sub-3-nm Technology Node. IEEE Transactions on Electron Devices, 2022, 69, 930-935.	1.6	8
3	Device Design Guidelines of 3-nm Node Complementary FET (CFET) in Perspective of Electrothermal Characteristics. IEEE Access, 2022, 10, 41112-41118.	2.6	4
4	LER-Induced Random Variation–Immune Effect of Metal-Interlayer–Semiconductor Source/Drain Structure on N-Type Ge Junctionless FinFETs. IEEE Transactions on Electron Devices, 2021, 68, 1340-1345.	1.6	1
5	Steep‣lope Gateâ€Connected Atomic Threshold Switching Field‣ffect Transistor with MoS <sub>2</sub> Channel and Its Application to Infrared Detectable Phototransistors. Advanced Science, 2021, 8, 2100208.	5.6	9
6	Enhancement of DRAM Performance by Adopting Metal–Interlayer–Semiconductor Source/Drain Contact Structure on DRAM Cell. IEEE Transactions on Electron Devices, 2021, 68, 2275-2280.	1.6	7
7	Enhancement of Synaptic Characteristics Achieved by the Optimization of Proton–Electron Coupling Effect in a Solid‣tate Electrolyteâ€Gated Transistor. Small, 2021, 17, e2100242.	5.2	13
8	Bimodal neural probe for highly co-localized chemical and electrical monitoring of neural activities in vivo. Biosensors and Bioelectronics, 2021, 191, 113473.	5.3	14
9	A minimally invasive flexible electrode array for simultaneous recording of ECoG signals from multiple brain regions. Lab on A Chip, 2021, 21, 2383-2397.	3.1	12
10	Electrothermal Characterization and Optimization of Monolithic 3D Complementary FET (CFET). IEEE Access, 2021, 9, 158116-158121.	2.6	6
11	Analysis of the Thermal Degradation Effect on a HfO <sub>2</sub> -Based Memristor Synapse Caused by Oxygen Affinity of a Top Electrode Metal and on a Neuromorphic System. ACS Applied Electronic Materials, 2021, 3, 5584-5591.	2.0	8
12	Improved switching characteristics of p-type tin monoxide field-effect transistors through Schottky energy barrier engineering. Journal of Materials Chemistry C, 2020, 8, 201-208.	2.7	17
13	A Hybrid RF MEMS Switch Actuated by the Combination of Bidirectional Thermal Actuations and Electrostatic Holding. IEEE Transactions on Microwave Theory and Techniques, 2020, 68, 3461-3470.	2.9	13
14	A Comprehensive Study on the Effect of TiN Top and Bottom Electrodes on Atomic Layer Deposited Ferroelectric Hf0.5Zr0.5O2 Thin Films. Materials, 2020, 13, 2968.	1.3	30
15	Hysteresis Modulation on Van der Waalsâ€Based Ferroelectric Fieldâ€Effect Transistor by Interfacial Passivation Technique and Its Application in Optic Neural Networks. Small, 2020, 16, e2004371.	5.2	35
16	Schottky barrier engineering with a metal nitride–double interlayer–semiconductor contact structure to achieve high thermal stability and ultralow contact resistivity. Applied Surface Science, 2020, 531, 147329.	3.1	0
17	A multiple negative differential resistance heterojunction device and its circuit application to ternary static random access memory. Nanoscale Horizons, 2020, 5, 654-662.	4.1	70
18	Analysis of Drain Linear Current Turn-Around Effect in Off-State Stress Mode in pMOSFET. IEEE Electron Device Letters, 2020, 41, 804-807.	2.2	6

#	Article	IF	CITATIONS
19	Nitrogen-Induced Enhancement of Synaptic Weight Reliability in Titanium Oxide-Based Resistive Artificial Synapse and Demonstration of the Reliability Effect on the Neuromorphic System. ACS Applied Materials & Interfaces, 2019, 11, 32178-32185.	4.0	25
20	Ultralow Schottky Barrier Height Achieved by Using Molybdenum Disulfide/Dielectric Stack for Source/Drain Contact. ACS Applied Materials & Interfaces, 2019, 11, 34084-34090.	4.0	6
21	Polarity control in a single transition metal dichalcogenide (TMD) transistor for homogeneous complementary logic circuits. Nanoscale, 2019, 11, 12871-12877.	2.8	21
22	Impact of Random Dopant Fluctuation on n-Type Ge Junctionless FinFETs With Metal–Interlayer–Semiconductor Source/Drain Contact Structure. IEEE Journal of the Electron Devices Society, 2019, 7, 1119-1124.	1.2	2
23	Infrared Detectable MoS <sub>2</sub> Phototransistor and Its Application to Artificial Multilevel Optic-Neural Synapse. ACS Nano, 2019, 13, 10294-10300.	7.3	96
24	Schottky barrier height modulation of metal–interlayer–semiconductor structure depending on contact surface orientation for multi-gate transistors. Applied Physics Letters, 2019, 114, 012102.	1.5	7
25	Schottky Barrier Height Modulation Using Interface Characteristics of MoS <sub>2</sub> Interlayer for Contact Structure. ACS Applied Materials & Interfaces, 2019, 11, 6230-6237.	4.0	19
26	Reduction of Threshold Voltage Hysteresis of MoS <sub>2</sub> Transistors with 3-Aminopropyltriethoxysilane Passivation and Its Application for Improved Synaptic Behavior. ACS Applied Materials & Interfaces, 2019, 11, 20949-20955.	4.0	19
27	Ultrathin EOT (0.67 nm) High-k Dielectric on Ge MOSFET Using Y Doped ZrO <sub>2</sub> With Record-Low Leakage Current. IEEE Electron Device Letters, 2019, 40, 502-505.	2.2	19
28	Nitrogen-Induced Filament Confinement Technique for a Highly Reliable Hafnium-Based Electrochemical Metallization Threshold Switch and Its Application to Flexible Logic Circuits. ACS Applied Materials & Interfaces, 2019, 11, 9182-9189.	4.0	28
29	Low-Temperature Hybrid Dopant Activation Technique Using Pulsed Green Laser for Heavily-Doped n-Type SiGe Source/Drain. IEEE Electron Device Letters, 2018, 39, 1828-1831.	2.2	4
30	Universal Metal-Interlayer-Semiconductor Contact Modeling Considering Interface-State Effect on Contact Resistivity Degradation. IEEE Transactions on Electron Devices, 2018, , 1-6.	1.6	2
31	Effective Schottky barrier height lowering technique for InGaAs contact scheme: DMIGS and Dit reduction and interfacial dipole formation. Applied Surface Science, 2018, 453, 48-55.	3.1	8
32	Schottky Barrier Height Engineering for Electrical Contacts of Multilayered MoS <sub>2</sub> Transistors with Reduction of Metal-Induced Gap States. ACS Nano, 2018, 12, 6292-6300.	7.3	130
33	Effects of Metal–Interlayer–Semiconductor Source/Drain Contact Structure on n-Type Germanium Junctionless FinFETs. IEEE Transactions on Electron Devices, 2018, 65, 3136-3141.	1.6	5
34	Novel Conductive Filament Metal–Interlayer–Semiconductor Contact Structure for Ultralow Contact Resistance Achievement. ACS Applied Materials & Interfaces, 2018, 10, 26378-26386.	4.0	5
35	Impact of Metal Nitrides on Contact Resistivity of Metal-Interlayer-Semiconductor Source/Drain in Sub-14 nm n-Type Si FinFET. Journal of Nanoscience and Nanotechnology, 2017, 17, 3084-3088.	0.9	1
36	Formation of Low-Resistivity Nickel Germanide Using Atomic Layer Deposited Nickel Thin Film. IEEE Transactions on Electron Devices, 2017, 64, 2599-2603.	1.6	14

#	Article	IF	CITATIONS
37	Fermi-Level Unpinning Technique with Excellent Thermal Stability for n-Type Germanium. ACS Applied Materials & Interfaces, 2017, 9, 35988-35997.	4.0	14
38	Investigation of Border Trap Characteristics in the AlON/GeO2/Ge Gate Stacks. IEEE Transactions on Electron Devices, 2017, 64, 3998-4001.	1.6	2
39	The Impact of an Ultrathin Y <sub>2</sub> O <sub>3</sub> Layer on GeO <sub>2</sub> Passivation in Ge MOS Gate Stacks. IEEE Transactions on Electron Devices, 2017, 64, 3303-3307.	1.6	19
40	Efficient Threshold Voltage Adjustment Technique by Dielectric Capping Effect on MoS <sub>2</sub> Field-Effect Transistor. IEEE Electron Device Letters, 2017, 38, 1172-1175.	2.2	13
41	Performance evaluation of 7nm n-type germanium junctionless field-effect-transistor with metal-interlayer-semiconductor source/drain structure. , 2017, , .		1
42	Fermi Level Depinning in Ti/GeO <sub>2</sub> /n-Ge via the Interfacial Reaction Between Ti and GeO <sub>2</sub> . IEEE Transactions on Electron Devices, 2017, 64, 4242-4245.	1.6	2
43	An Electrical Analysis of a Metal-Interlayer-Semiconductor Structure on High-Quality Si1â^'x Gex Films for Non-Alloyed Ohmic Contact. Journal of Nanoscience and Nanotechnology, 2017, 17, 7323-7326.	0.9	0
44	2-Dimensional Analysis of Plasma Ashing Damage Induced by Oxygen-Based Plasmas Along Nanopores in SiOCH Film for a Nanoscale Back-End of Line Process. Journal of Nanoscience and Nanotechnology, 2016, 16, 11766-11770.	0.9	0
45	The Effect of Interfacial Dipoles on the Metal-Double Interlayers-Semiconductor Structure and Their Application in Contact Resistivity Reduction. ACS Applied Materials & Interfaces, 2016, 8, 35614-35620.	4.0	24
46	The Effect of Post-Fabrication Annealing on an Amorphous IGZO Visible-Light Photodetector. Journal of Nanoscience and Nanotechnology, 2016, 16, 11745-11749.	0.9	3
47	Contact Resistance Reduction Using Dielectric Materials of Nanoscale Thickness on Silicon for Monolithic 3D Integration. Journal of Nanoscience and Nanotechnology, 2016, 16, 12764-12767.	0.9	5
48	Effective Schottky Barrier Height Lowering of Metal/n-Ge with a TiO <sub>2</sub> /GeO <sub>2</sub> Interlayer Stack. ACS Applied Materials & Interfaces, 2016, 8, 35419-35425.	4.0	37
49	Threshold voltage variation-immune FinFET design with metal-interlayer-semiconductor source/drain structure. Current Applied Physics, 2016, 16, 618-622.	1.1	2
50	Effect of Metal Nitride on Contact Resist ivity of Metal- Interlayer- Ge Source/Drain in Sub- 10 nm ntype Ge FinFET. IEEE Electron Device Letters, 2016, , 1-1.	2.2	3
51	Effect of Hydrogen Annealing on Contact Resistance Reduction of Metal–Interlayer–n-Germanium Source/Drain Structure. IEEE Electron Device Letters, 2016, , 1-1.	2.2	11
52	Random Dopant Fluctuation-Induced Threshold Voltage Variation-Immune Ge FinFET With Metal–Interlayer–Semiconductor Source/Drain. IEEE Transactions on Electron Devices, 2016, 63, 4167-4172.	1.6	14
53	Extremely Low Contact Resistance on Graphene through nâ€Type Doping and Edge Contact Design. Advanced Materials, 2016, 28, 864-870.	11.1	70
54	A Highâ€Performance WSe <sub>2</sub> / <i>h</i> â€BN Photodetector using a Triphenylphosphine (PPh <sub>3</sub> )â€Based nâ€Đoping Technique. Advanced Materials, 2016, 28, 4824-4831.	11.1	139

#	Article	IF	CITATIONS
55	Graphene: Extremely Low Contact Resistance on Graphene through nâ€Type Doping and Edge Contact Design (Adv. Mater. 5/2016). Advanced Materials, 2016, 28, 975-975.	11.1	2
56	Non-Alloyed Ohmic Contacts on GaAs Using Metal-Interlayer-Semiconductor Structure With SF <sub>6</sub> Plasma Treatment. IEEE Electron Device Letters, 2016, 37, 373-376.	2.2	11
57	Theoretical and Experimental Investigation of Graphene/High-k/p-Si Junctions. IEEE Electron Device Letters, 2016, 37, 4-7.	2.2	5
58	Photodetectors: Highâ€Performance Transition Metal Dichalcogenide Photodetectors Enhanced by Selfâ€Assembled Monolayer Doping (Adv. Funct. Mater. 27/2015). Advanced Functional Materials, 2015, 25, 4368-4368.	7.8	1
59	Highâ€Performance Transition Metal Dichalcogenide Photodetectors Enhanced by Selfâ€Assembled Monolayer Doping. Advanced Functional Materials, 2015, 25, 4219-4227.	7.8	247
60	Negative Capacitance in Organic/Ferroelectric Capacitor to Implement Steep Switching MOS Devices. Nano Letters, 2015, 15, 4553-4556.	4.5	162
61	Fermi-Level Unpinning Using a Ge-Passivated Metal–Interlayer–Semiconductor Structure for Non-Alloyed Ohmic Contact of High-Electron-Mobility Transistors. IEEE Electron Device Letters, 2015, 36, 884-886.	2.2	12
62	The Mechanism of Schottky Barrier Modulation of Tantalum Nitride/Ge Contacts. IEEE Electron Device Letters, 2015, 36, 997-1000.	2.2	21
63	Surface Passivation of Germanium Using SF <sub>6</sub> Plasma to Reduce Source/Drain Contact Resistance in Germanium n-FET. IEEE Electron Device Letters, 2015, 36, 745-747.	2.2	23
64	The Efficacy of Metal-Interfacial Layer-Semiconductor Source/Drain Structure on Sub-10-nm n-Type Ge FinFET Performances. IEEE Electron Device Letters, 2014, 35, 1185-1187.	2.2	19
65	Specific Contact Resistivity Reduction Through Ar Plasma-Treated TiO <sub>2â^'x</sub> Interfacial Layer to Metal/Ge Contact. IEEE Electron Device Letters, 2014, 35, 1076-1078.	2.2	34
66	Analytical Study of Interfacial Layer Doping Effect on Contact Resistivity in Metal-Interfacial Layer-Ge Structure. IEEE Electron Device Letters, 2014, 35, 705-707.	2.2	22
67	Dopant profile model in a shallow germanium n+/p junction. Journal of the Korean Physical Society, 2013, 63, 1855-1858.	0.3	0
68	Electrical properties of phosphorus-doped polycrystalline germanium formed by solid-phase and metal-induced crystallization. Journal of Alloys and Compounds, 2013, 561, 231-233.	2.8	36
69	Characteristics of Ultrashallow Hetero Indium–Gallium–Zinc–Oxide/Germanium Junction. IEEE Electron Device Letters, 2012, 33, 1363-1365.	2.2	2
70	Selective-Area High-Quality Germanium Growth for Monolithic Integrated Optoelectronics. IEEE Electron Device Letters, 2012, 33, 579-581.	2.2	18